Electron capture to D_3^- and D_3^0 repulsive states by D_3^+ in Cs

C. Cisneros, I. Alvarez, and R. García G.
Instituto de Física, Universidad Nacional Autonoma de Mexico, Mexico 20, D.F.

C. F. Barnett and J. A. Ray
Oak Ridge National Laboratory, Oak Ridge, Tennessee 37830

A. Russek
The University of Connecticut, Storrs, Connecticut 06268

(Received 14 April 1978)

Differential cross sections for the production of D^- and $D^0 + D_2^0 + D_3^0$ are given for electron-capture collisions into D_3^- and D_3^0 repulsive states by bombardment of Cs with D_3^+ ions in the energy range 1.5–7.5 keV. A theory is presented for the angular distributions of dissociation fragments in the special cases in which the dissociation (i) produces two fragments, or (ii) produces three fragments, one of which has a small energy in the molecular center-of-mass frame. In both cases a scaling law is predicted: $(\gamma_n E_i)^{-1}\, d\sigma_n/d\omega = f(\gamma_n E_i \theta_n^2)$, where $d\sigma_n/d\omega$ is the differential cross section for finding fragment n at angle θ_n, E_i is the incident energy, and γ_n is a mass ratio. The D^- distributions are observed to fit this scaling law. Peaks are found in both the D^- and $D^0 + D_2^0 + D_3^0$ distributions for which $1/2E_i\theta^2 \simeq 15$ keV deg^2 and 14 keV deg^2, respectively. A corresponding peak is also found in the neutral distribution for which $2E_i\theta^2 \simeq 14$ keV deg^2. The peaks indicate a repulsive state in D_3^- which decays into $D^- + D_2^0$, and a repulsive state in D_3^0 which decays into $D^0 + D_2^0$ and which has an energy surface close to that of the D_3^- repulsive state. An energy surface of a repulsive singlet state of D_3^- is presented which does decay into D^- and D_2^0.

I. INTRODUCTION

In a previous work,[1] measurements were reported on the angular distributions of dissociation fragments which result from one- and two-electron capture by D_2^+ to repulsive states of D_2^- and D_2^0. (D_2^+ was used as the incident projectile because the experiments were motivated by an interest in D^- formation for use in injection heating of a thermonuclear plasma.[2,3] However, all results, both experimental and theoretical, hold as well for H_2^+ as for D_2^+.) In addition, the theory of the angular distribution was presented which indicated that a scaling law

$$\frac{1}{E_i}\frac{d\sigma_n}{d\omega} = f(E_i\theta^2)$$

should hold, where $d\sigma_n/d\omega$ is the differential cross section for fragment n, E_i is the energy of the incident D_2^+ ion, and θ is the angle between the observed fragment and the incident beam direction. Since the electron-capture process causes a negligible deflection, this angular deflection is entirely due to the transverse component of the dissociation velocity $\vec{v}_d$ of the fragment. The scaling law was experimentally verified and provided a powerful tool for checking consistency in the experimental results.

In the present work both the experiment and the theory are extended to single- and double-electron-capture processes by the triatomic molecular ion D_3^+. Again, H_3^+ could equally well have been used in the experiment. In particular, the theory has been extended to the two-fragment dissociation of a triatomic molecular system and to the three-fragment dissociation where one of the fragments has a negligible dissociation velocity in the molecular center-of-mass frame. A scaling law is predicted for each of these two important cases.

In Sec. II, the apparatus and experimental procedures are briefly described, while Sec. III presents the experimental results. In Sec. IV, the theory of angular distribution of dissociation fragments is generalized to cover the case of breakup into fragments of unequal masses, and the data of Sec. III are analyzed in terms of the scaled variables.

II. APPARATUS AND MEASUREMENTS

A. General description

Figure 1 shows the experimental arrangement, which has been described previously.[2] A D_3^+ beam is generated in a Von-Ardenne-type ion source, accelerated to the desired energy, magnetically focused, and mass analyzed. The mass- and velocity-analyzed beam passes through additional ion optics and enters the collision cell, which is filled with Cs vapor at very low pressure to assure single collisions. The Cs vapor density is determined from the oven temperature, using the vapor pressure-temperature curves for Cs

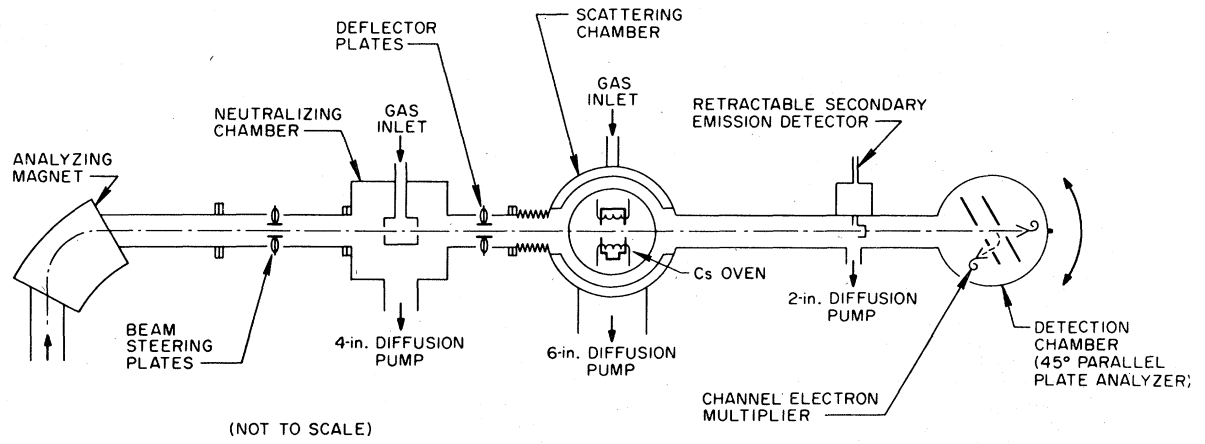

FIG. 1. Schematic diagram of the apparatus.

vapor.[2,4,5] The details of the collision cell and the Cs oven are given in Ref. 2.

The Cs cell geometry permits the measurement of the angles made by dissociation fragments with respect to the incident beam direction, up to angles of $\pm 7°$. The detector assembly can be rotated about the center of the scattering chamber to obtain angular distributions. Pathlengths and apertures were chosen such that the root mean square of the angular resolution of the system is $0.1°$.

The dissociation fragment then enters at $45°$ a parabolic electrostatic analyzer[6] that employs separate multipliers for the neutral and ion components of the beam. The multiplier counting efficiencies for D^- and D^+ have been determined previously[7] and have been used to correct the experimental data in this work.

B. Procedure

The procedure was the same as that described in Ref. 1. The measured quantities were I_0, the number of D_3^+ ions incident per unit of area per second; n, the number of Cs atoms per unit volume; l, the effective length of the scattering chamber; and $I_f(\theta)$, the number of fragments of type f (where f stands for D^- or $D_3^0 + D_2^0 + D^0$) per unit solid angle per second detected at angle θ with respect to the incident beam direction. With these measurements, the quantity

$$\frac{d\sigma_f}{d\omega} = \frac{I_f(\theta)}{I_0 n l} \tag{1}$$

was calculated. As Ref. 1 points out, although $d\sigma_f/d\omega$ formally looks like a differential cross section and is measured like one, the fragment detected at angle θ has not been "scattered." The substantial angle at which a fragment is found is due to the transverse component of the velocity acquired in the dissociation process.

Several sources of error are present in each of the measured quantities and have been discussed in previous papers.[1,2] These involve the effective length of the gas cell, the measurement of the incident ion current, the absolute-density determination, the angular resolution, and the detector calibration. Although data were corrected to account for most of these uncertainties, a total error of $\pm 30\%$ in the final data has been estimated.

III. RESULTS

Angular distributions of D^- formed from single collisions of D_3^+ on Cs at collision energies of 1.5, 3.0, 4.5, 6.0, and 7.5 keV were obtained by setting the energy analyzer in the detector assembly at $\frac{1}{3}$ of the total D_3^+ incoming beam energy. Figure 2 shows $d\sigma/d\omega$ obtained from the measured angular distributions using Eq. (1).

At 1.5-, 3-, 4.5-, and 7.0-keV incident energies, angular distributions were also taken for $D^0 + D_2^0 + D_3^0$. Figure 3 shows these results. It was not possible to separate each of the three components from the total neutral component. However, it may be confidently expected that the D_3^0 component will be found only at very small angles.[2] As is discussed below, the D_2^0 component is expected to be responsible for the first peak in the neutral angular distributions, while the second peak in the neutral angular distribution is due to D^0 only. It is interesting to note that the first peak appears at half of the angle of the second one for all the energies at which runs were made. Figure 4 shows the results for D_3^+ incoming beam energy of 4.5 keV.

Previous investigations[8,9] have shown that H^+ formation cross sections from dissociative collisions were dependent upon the ion source parameters. Williams and Dunbar[9] found similar results for the production of H^- from H_2^+ passing

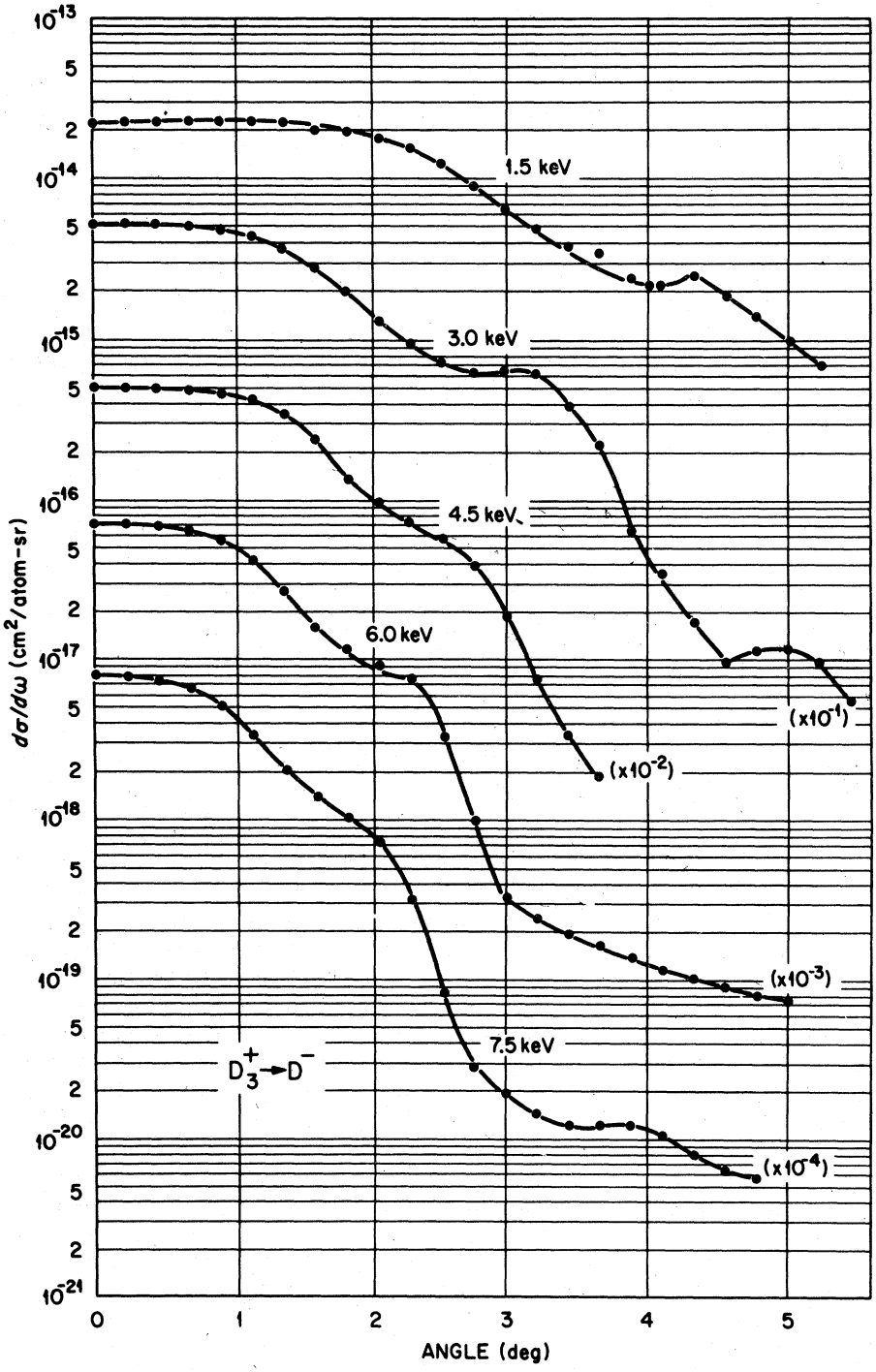

FIG. 2. Differential cross sections for the formation of D^- for 1.5−, 3.0−, 4.5−, 6.0−, and 7.5 − keV D_3^+ incident on cesium vapor.

through H_2. These studies have shown that the cross sections could be dependent on the state of vibrational excitation of the ion prior to the collision. In the present work changes were observed in the absolute values with respect to the ion source conditions. Consequently, great care was taken to use the same ion source parameters in all runs. When this was done, the cross sections were reproducible to within 15%. All data were taken at a target density of 2.56×10^{13} atoms/cm^2.

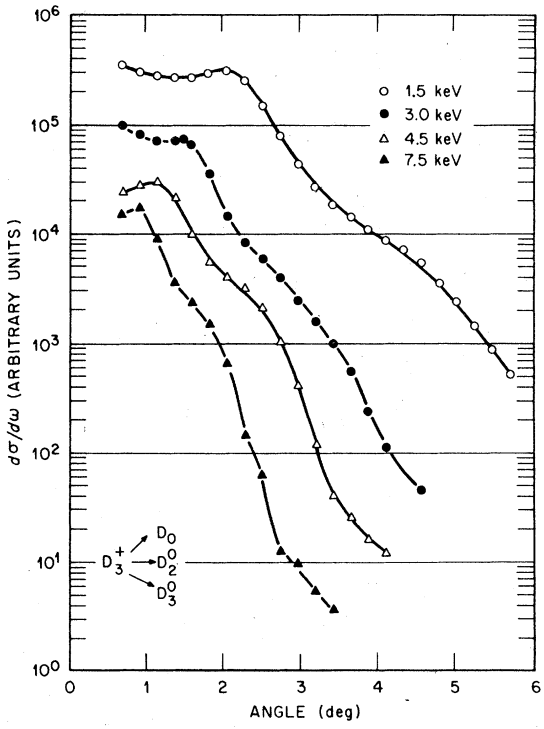

FIG. 3. Differential cross sections for the formation of $D^0 + D_2{}^0 + D_3{}^0$ for 1.5 –, 3.0 –, 4.5 –, and 7.5 – keV D_3^+ incident on cesium vapor. In the present experiment the individual constitutents in the neutral beam were not separated.

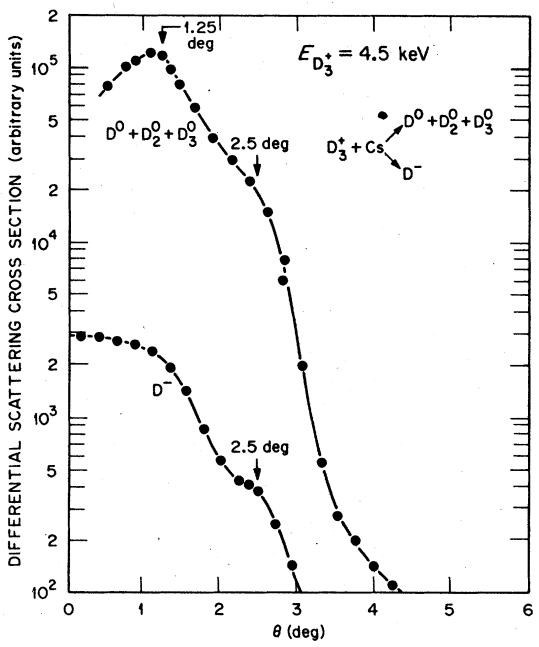

FIG. 4. Differential cross sections for the formation of D^- and for the formation of $D^0 + D_2{}^0 + D_3{}^0$ for 4.5 – keV D_3^+ incident on cesium vapor.

IV. THEORY OF THE ANGULAR DISTRIBUTION

In Ref. 1, a theory of fragment angular distributions produced by molecular dissociations was derived for the special case of a homonuclear binary molecule. The theory is, however, easily generalized to cover diatomic molecules for which the masses are not equal and to describe the dissociation of a polyatomic molecule into two fragments. The generalized theory is based on the same five assumptions that were made in Ref. 1. (i) The capture process is fast compared with the periods of both vibrational and rotational motion. The incident molecule can therefore be considered to have a fixed orientation and a fixed geometry during the electron capture process. (ii) Rotational energies are negligible compared with dissociation energies, so that the dissociation direction is that of the line joining the two fragments. (iii) All orientations are equally probable. (iv) Dissociation velocities are very small compared with incident beam velocities. (v) The center of mass of the molecular ion suffers a negligible deflection due to the electron-capture process. Thus the angular difference between the direction of motion of a fragment and the incident beam direction is due entirely to the transverse component of the velocity of the dissociating fragments.

The first part of the derivation follows rather closely the derivation given in Ref. 1 and will be discussed only briefly here. Let $\vec{v}_A$ and $\vec{v}_B$ be the dissociation velocities of fragments m_A and m_B in the molecular center-of-mass frame of the molecule AB. Either of these quantities may be a composite system, provided that it does not itself dissociate before detection. (The detector, of course, is insensitive to the system's center of mass; it detects only particles.) In the following treatment A denotes a D^- fragment, and B denotes a $D_2{}^0$ fragment in the dissociation of $D_3{}^-$. In the molecular center-of-mass frame, the dissociation energy E_d is equal to

$$E_d = \tfrac{1}{2} m_A v_A^2 + \tfrac{1}{2} m_B v_B^2 , \tag{2}$$

where conservation of momentum requires that

$$m_A \vec{v}_A = -m_B \vec{v}_B . \tag{3}$$

It should be noted that E_d is the kinetic energy of the dissociating fragments. If a fragment is composite, it will generally have a vibrational-rotational energy E_v, which must be taken into account in the energy equation. Thus, for example, in the dissociation $D_3{}^- \rightarrow D^- + D_2{}^0$, we have

$$E_{D_3^-} = E_{D^-} + E_{D_2{}^0} + E_v + E_d .$$

It easily follows from (2) and (3) that

$$v_A = \left(\frac{2E_d}{m_A+m_B}\frac{m_B}{m_A}\right)^{1/2} \tag{4a}$$

and

$$v_B = \left(\frac{2E_d}{m_A+m_B}\frac{m_A}{m_B}\right)^{1/2}. \tag{4b}$$

Since

$$E_i = \tfrac{1}{2}(m_A+m_B)v_i^2, \tag{5}$$

where E_i and v_i are the energy and velocity of the incident ion in the laboratory, Eqs. (4a) and (4b) yield the relations

$$(v_i/v_A)^2 = (m_A/m_B)(E_i/E_d), \tag{6a}$$

and

$$(v_i/v_B)^2 = (m_B/m_A)(E_i/E_d), \tag{6b}$$

needed in the derivation which follows. Assuming that dissociation velocities are very small compared with the incident beam velocity, we can determine, from the same approximations described in Ref. 1, that in the laboratory frame the directions of fragments A and B relative to the incident beam direction are given by

$$\theta_A \simeq \sin\theta_A \simeq (v_A/v_i)\sin\Theta = \left(\frac{m_B}{m_A}\frac{E_d}{E_i}\right)^{1/2}\sin\Theta \tag{7a}$$

and

$$\theta_B \simeq \sin\theta_B \simeq (v_B/v_i)\sin\Theta = \left(\frac{m_A}{m_B}\frac{E_d}{E_i}\right)^{1/2}\sin\Theta \tag{7b}$$

with

$$\phi_B = \pi + \phi_A = \Phi. \tag{8}$$

Here θ is the angle made by the vector $\vec{R}_3 = \vec{R}_A - \vec{R}_B$ with the incident beam direction (see Fig. 5), and Φ is the azimuthal angle of the projection of $\vec{R}_3$ in the plane perpendicular to the beam direction.

The relationship between the differential solid angles is easily derived[1] from Eqs. (7) and (8):

$$d\Omega = \frac{m_A}{m_B}\frac{E_i}{E_d}\,d\omega_A/[1-(m_A/m_B)E_i\theta_A^2/E_d]^{1/2}$$
$$= \frac{m_B}{m_A}\frac{E_i}{E_d}\,d\omega_B/[1-(m_B/m_A)E_i\theta_B^2/E_d]^{1/2}, \tag{9}$$

where Ω (i.e., Θ and Φ) describes the orientation of the molecular ion at the time of electron capture and where $\vec{\omega}_A$ and $\vec{\omega}_B$ (i.e., θ_A, ϕ_A, θ_B, and ϕ_B) are the angles at which the fragments A and B are found in the laboratory frame of reference. An exact treatment of the relation between the differential solid angles in the center of mass and the laboratory frames, not restricted to small θ and $E_d/E_i \ll 1$, can be found in Fluendy and Lawley.[10]

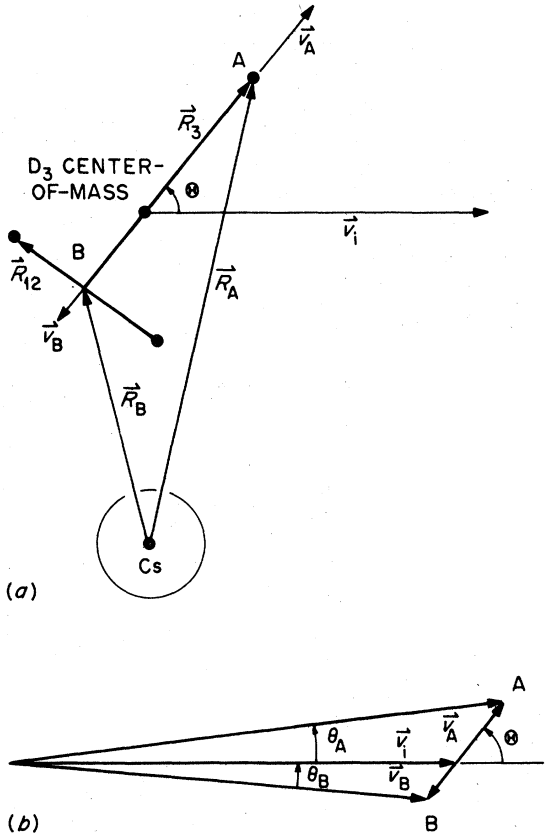

FIG. 5. (a) Schematic diagram of the collision showing the coordinate system. Also shown are the fragment dissociation velocities $\vec{v}_A$ and $\vec{v}_B$. (b) Velocity diagram showing the relation between the angle θ in the molecular reference frame and the angles θ_A and θ_B of fragments A and B in the laboratory frame.

The number of fragments dN_A of type A found in the differential solid angle $d\Omega$ in the molecular center-of-mass frame is proportional both to the number of projectiles N and the number of targets N_t per unit area. It is also proportional to the cross section σ_c for the appropriate electron-capture process, which is a function of both molecular shape and orientation as the projectile passes by the target. Because the orientation angle Φ is averaged over in the experiment, the cross section σ_c used here will also be averaged over all azimuthal directions Φ of the vector $\vec{R}_3$. Thus

$$dN_A = NN_t \int dR_{12} \int dR_3\, \rho(R_{12}, R_3) \times \sigma_c(R_{12}, R_3, \Theta)\, d\Omega/4\pi, \tag{10}$$

where $\rho(R_{12}, R_3)\,dR_{12}\,dR_3$ gives the probability that the molecular configuration lies in the range $dR_{12}\,dR_3$, and $d\Omega/4\pi$ gives the probability that the

orientation of $\vec{R}_3$ lies in $d\Omega$ at the time of passage. Since neither R_{12} nor R_3 is measured in this experiment, both must be integrated over the entire range of R_{12} and R_3.

Equation (10) gives the angular distribution of fragments in the molecular center-of-mass system. However, the angular distribution in the laboratory frame is desired, so the transformation (9) must be used to yield

$$dN_A = \frac{NN_t}{4\pi}\int dR_{12}\int dR_3\,\rho(R_{12},R_3)\sigma_c(R_{12},R_3,\Theta) \times \frac{m_A}{m_B}\frac{E_i}{E_d^{1/2}}\frac{d\omega_A}{[E_d-(m_A/m_B)E_i\theta_A^2]^{1/2}}. \tag{11}$$

In order to facilitate comparison with experiment, a "cross section" is defined:

$$\frac{d\sigma_A}{d\omega} = \frac{1}{NN_t}\frac{dN_A}{d\omega_A} = \frac{I_A(\theta)}{I_0 nl}. \tag{12}$$

With the definition (12), (11) becomes, after dividing through by $NN_t(m_A/m_B)E_i d\omega_A$:

$$\frac{m_B}{m_A}\frac{1}{E_i}\frac{d\sigma_A}{d\omega} = \frac{1}{4\pi}\int dR_{12}\int dR_3\,\frac{\rho(R_{12},R_3)\sigma_c(R_{12},R_3,\Theta)}{E_d^{1/2}(E_d-(m_A/m_B)E_i\theta_A^2)^{1/2}} = f((m_A/m_B)E_i\theta_A^2). \tag{13a}$$

The integration is understood over the entire range of R_{12} and R_3 for which $E_d \geq (m_A/m_B)E_i\theta_A^2$, remembering that the dissociation energy E_d is a function of both R_{12} and R_3.

In a similar manner, the angular distribution of fragment B is found to be

$$\frac{m_A}{m_B}\frac{1}{E_i}\frac{d\sigma_B}{d\omega} = \frac{1}{4\pi}\int dR_{12}\int dR_3\,\frac{\rho(R_{12},R_3)\sigma_c(R_{12},R_3,\Theta)}{E_d^{1/2}[E_d-(m_B/m_A)E_i\theta_B^2]^{1/2}} = f((m_B/m_A)E_i\theta_B^2). \tag{13b}$$

A consequence of Eqs. (13a) and (13b) is that if fragments A and B come from the same decay channel, the curves $Y_A = f(X_A)$ and the curves $Y_B = f(X_B)$ must be identical, where

$$X_A = \frac{m_A}{m_B}E_i\theta_A^2, \quad X_B = \frac{m_B}{m_A}E_i\theta_B^2; \qquad Y_A = \frac{m_B}{m_A}\frac{1}{E_i}\frac{d\sigma_A}{d\omega}, \quad Y_B = \frac{m_A}{m_B}\frac{1}{E_i}\frac{d\sigma_B}{d\omega}. \tag{14}$$

It also follows from Eqs. (13a) and (13b) that a peak in the fragment A distribution at angle θ_A should be associated with a peak in the fragment B distribution at angle θ_B, where

$$\frac{m_A}{m_B}E_i\theta_A^2 = \frac{m_B}{m_A}E_i\theta_B^2,$$

or more compactly written,

$$\theta_A/\theta_B = m_B/m_A. \tag{15}$$

It further follows that the peak heights (above backgrounds due to other processes) should be in the ratios

$$h_A/h_B = m_A^2/m_B^2. \tag{16}$$

Two special cases are of interest in this work. Case A: $D_3^- \rightarrow D^- + D_2^0$ or $D_3^0 \rightarrow D^0 + D_2^0$. For both of these dissociations, m_A/m_B equals $\frac{1}{2}$, where A represents the D^- or D^0 fragment and B represents the D_2^0 fragment.

$$\theta_A = 2\theta_B, \quad X_A = \tfrac{1}{2}E_i\theta_A^2, \quad Y_A = \frac{2}{E_i}\frac{d\sigma_A}{d\omega}; \qquad h_B = 4h_A, \quad X_B = 2E_i\theta_B^2, \quad Y_B = \frac{1}{2E_i}\frac{d\sigma_B}{d\omega}. \tag{17}$$

Case B: One of the fragments C acquires a negligible velocity in a three-particle dissociation: $D_3^- \rightarrow D^0 + D^0 + D^-$ or $D_3^0 \rightarrow D^0 + D^0 + D^0$. For both of these dissociations, $m_A = m_B$, so that

$$\theta_A = \theta_B, \quad \theta_C = 0, \quad h_A = h_B, \quad X_A = X_B = E_i\theta^2, \text{ where } \theta = \theta_A \text{ or } \theta_B, \quad Y_A = Y_B = \frac{1}{E_i}\frac{d\sigma}{d\omega}. \tag{18}$$

The negative-ion data in Fig. 2 are replotted in terms of the scaled variables in Fig. 6. In this case, the angular distributions followed the scaling law previously discussed. As in the case of D_2^+ studies,[1] a monotonically decreasing contribution, possibly from other processes, was assumed and such contribution was subtracted as background. Figure 7 shows the peak plotted in terms of the scaled variables $\frac{1}{2}E_i\theta^2$ with the background subtracted out. In this case, absolute values for the reduced differential cross sections were calculated, since all the quantities which appear in Eq. (1) are known, as well as detector efficiencies for all the energies.[7] In the energy range studied, Figs. 6 and 7 clearly show that the capture process which leads to D^- is independent of velocity. This is in accord with molecular theory in this energy range. Basically, the process has a large probability if the impact parameter is less than the appropriate level-crossing radius and has essentially zero probability otherwise, independent of the velocity. At high incident velocities, however, this approximation is

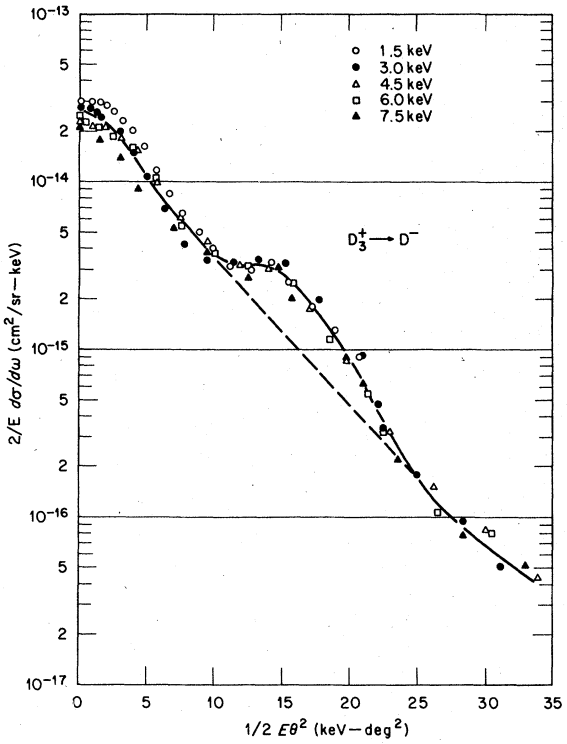

FIG. 6. Figure 2 replotted in terms of the reduced variables $\frac{1}{2}E_i\theta^2$ for the abscissa and $(2E_i)^{-1}d\sigma_-/d\omega$ for the ordinate, in accordance with Eqs. (17).

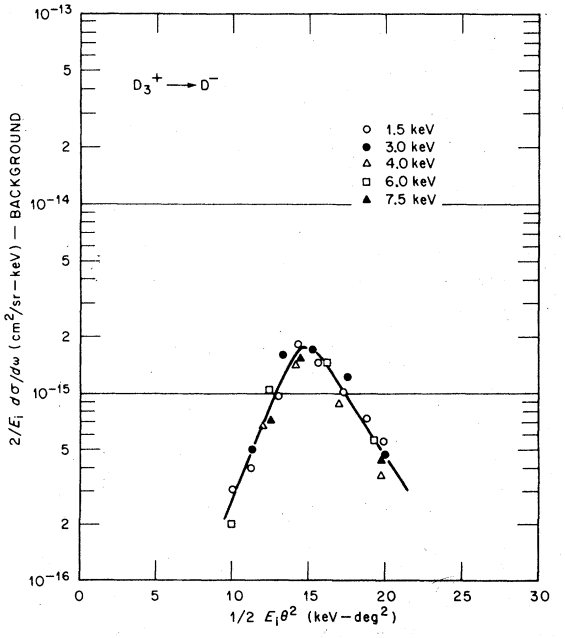

FIG. 7. Reduced cross section of Fig. 6 with the background subtracted out.

expected to break down.

The neutral angular distributions were treated in the same way: monotonically decreasing contributions from other processes were assumed. The two different peaks which appear in the angular distributions shown in Fig. 2 were isolated after the background subtraction. As Eqs. (17) show, no single scaling law applies. Fragments with different masses scale differently. In the case of the D^0 products which appear at the larger angles, it was possible to calculate the absolute differential cross sections. However, an extra source of error has to be taken in account: the detector efficiency was not directly determined. A rough approximation was made, and the detector efficiency was taken to be between that measured for D^+ and for D^- in Ref. 7. Figure 8 shows the results for the neutral case. It can be seen from this figure that the reduced curves have similar shapes: they all show a peak at $\frac{1}{2}E\theta^2 = 14$ keV deg^2, but the heights change with the incident energy. From this fact, it is possible to conclude that the main process which leads to D^0 background is velocity dependent, as opposed to the D^- curves which scale completely, background and all. Because the height of the scaled D^- curve is about one order of magnitude lower than that of D^0, it cannot at this time be completely ruled out that the D^- could come from a three-body decomposition with one slow D^0 and one fast D^0 at the same laboratory angle as the D^-. This possibility would yield a component to the D^0 distribution slightly shifted from the observed distribution. However, because it would be so small, it could be missed. Nevertheless, the most likely conclusion from the data is that electron capture to repulsive D_3^0 states and D_3^- states occurs in a ratio which lies between 10 to 1 and 50 to 1 and that both repulsive states decay into a D_2^0, with the other fragment being a D^0 or D^-. In the case of D_2^0 the absolute value of the differential cross section, $d\sigma/d\omega$, was not calculated, since the peak appears at very small angles. In this angular region, a large error can be introduced, since the overall neutral component will be a mixture of D_2^0 plus D^0 at half of the energy and the data cannot be properly corrected for the detector efficiency. However, the peak position $2E_i\theta^2 \simeq 14$ keV deg^2 shows a contribution of D_2^0 coming together with D^0 from the dissociation of D_3^0. Figure 9 shows the two neutral peaks. The one that appears at small angles is plotted as a function of $2E\theta^2$, and the one that appears at greater angles plotted as a function of $\frac{1}{2}E\theta^2$, according to the scaling law for a $D_2^0 + D^0$ dissociation. Both are normalized to have the same height. As is seen from Fig. 9, the peak which has the D_2^0 con-

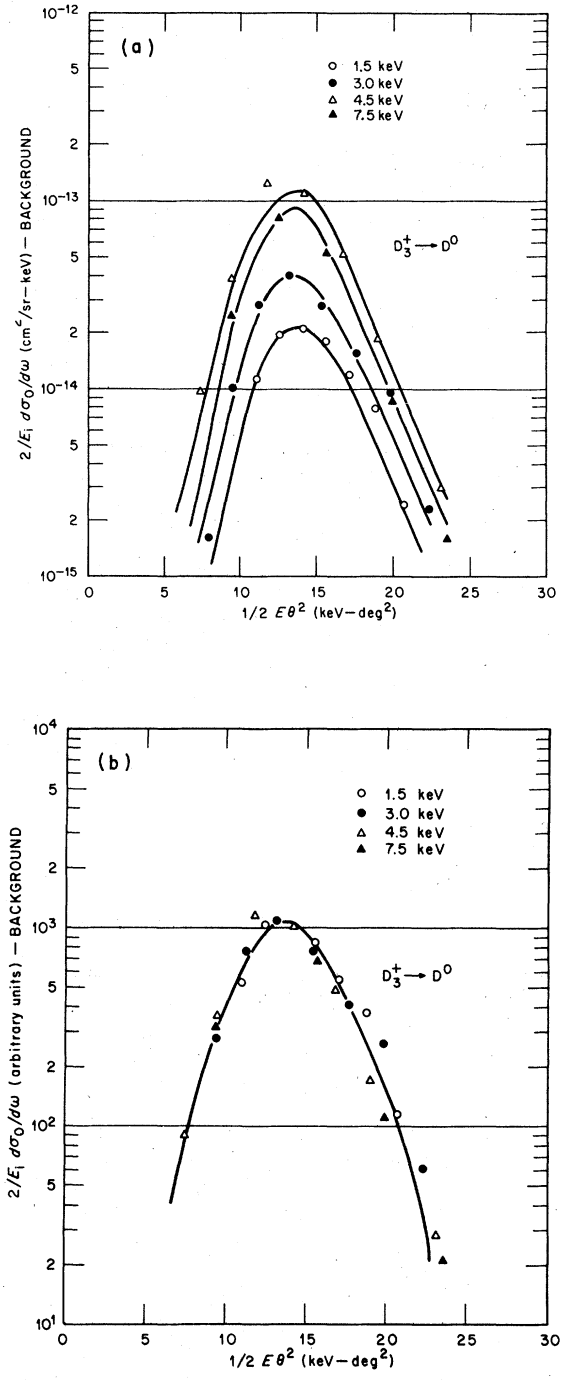

FIG. 8. (a) Peaks in Fig. 3 replotted after the background has been subtracted out. The peaks are plotted here in terms of the reduced variables $\frac{1}{2}E_i\theta^2$ for the abscissa and $(2E)^{-1}d\sigma_0/d\omega$ for the ordinate, in accordance with Eqs. (17). The difference in heights of these peaks is most probably due to inaccuracy in background subtraction. (b) Peaks in (a) normalized to the same peak height, on the assumption that the differences in peak heights are due to inaccuracy of background subtraction.

tribution is wider than the corresponding D^0 peak. A possible reason for the anomalous width of this peak is that it contains contributions from other processes in addition to some D^0. The rather difficult problem of properly subtracting the "background" makes the experimental results too uncertain to draw any definite conclusions. To support the contention that the observed D^- comes from the dissociation $D_3^- \rightarrow D^- + D_2^0$, the lowest singlet dissociating state of D_3^-, taken from García G. *et al.*,[11] is shown in Fig. 10. The equilibrium configuration of the incident D_3^+ ion is indicated by an $\times$. In its equilibrium configuration this state clearly dissociates into $D^- + D_2^0$, each in its respective ground electronic states, but with D_2^0 in a distribution of excited vibrational states.

A peak in the distribution for any given fragment is due to the singularity in the Jacobian of the transformation (9), which relates the differential solid angle in the center-of-mass frame to that in the laboratory.[10,12] It occurs when

$$1 - \gamma E_i \theta^2 / E_d = 0 , \tag{19}$$

where γ is the mass of the detected fragment divided by the mass of the other fragment. Using (19), the dissociation energy can be determined from the location of the peak in the fragment angular distribution:

$$E_d = \gamma E_i \theta_{\text{peak}}^2 . \tag{20}$$

Equation (20), which is valid when θ_{peak} is small and $E_d/E_i \ll 1$, is an approximation to the exact

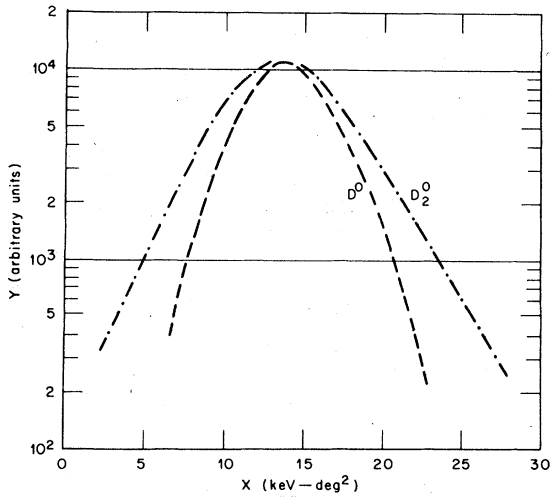

FIG. 9. The D_2^0 and D^0 peaks plotted in terms of the scaled variables given in Eqs. (17). The D^0 peak is taken from Fig. 8 (b). The D_2^0 peak is normalized to have the same height as the D^0 peak, on the assumption that differences in peak heights are most probably due to inaccuracy in background subtraction.

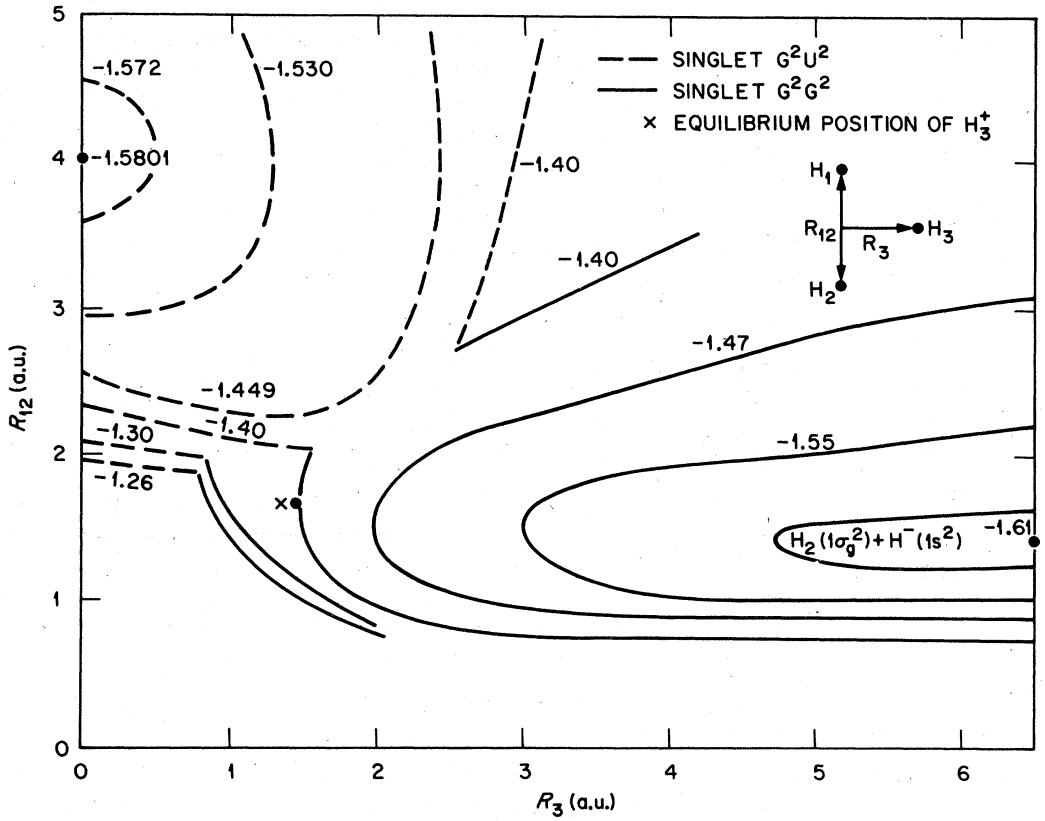

FIG. 10. Energy surface at the lowest repulsive singlet state taken from García *et al.*[10] The solid and dashed lines are energy contours in atomic units (1 a.u. = 27.2 eV). This surface shows a bound H_3^-(or D_3^-) state at −1.58 a.u. and a dissociated H_2 $(1\sigma g^2)+H^-$ $(1s^2)$ state at −1.61 a.u. The equilibrium configuration of the incident D_3^+ ion is indicated by an ×.

result[10,12]

$$\theta_{\text{peak}} = \sin^{-1}(E_d/\gamma E_i)^{1/2}. \tag{21}$$

From Fig. 10 it can be seen that if H_3^- is formed approximately at the equilibrium configuration of the incident H_3^+ ion, then the maximum energy which can be liberated is 0.21 a.u. (i.e., 1.61 − 1.40) or 5.7 eV. The dissociation energy E_d will be less if the H_2 is vibrationally excited in the dissociation process. On the other hand, from Fig. 7 it can be seen that the peak in the angular distribution occurs when $\gamma E_i\theta^2 = 15$ keV deg^2, which yields a value 4.6 eV for E_d, indicating that the H_2 fragment emerges with approximately 1.1 eV of vibrational plus rotational energy.

ACKNOWLEDGMENTS

The experimental work was supported by the Division of Magnetic Fusion Energy, U. S. Department of Energy, under Contract No. W-7405-eng-26 with the Union Carbide Corporation. The theory and analysis was supported by a joint grant from the Latin American Cooperative program of NSF (U.S.A.) and CONACYT (Mexico): NSF-PNCB-CONACYT No. 1367.

[1]C. Cisneros, I. Alvarez, C. F. Barnett, J. A. Ray, and A. Russek, Phys. Rev. A 14, 88 (1976).

[2]C. Cisneros, I. Alvarez, C. F. Barnett, and J. A. Ray, Phys. Rev. A 14, 76 (1976).

[3]Atomic, Molecular and Nuclear Data Needs for C.T.R., U. S. Energy Research and Development Administration Report No. 39 (unpublished).

[4]L. L. Marino, A. C. H. Smith, and E. Caplinger, Phys. Rev. 128, 2243 (1962).

[5]R. H. Hultgren, R. L. Onn, P. D. Anderson, and K. K. Kelley, *Selected Values of Thermodynamic Properties of Metals and Alloys* (Wiley, New York, 1963), p. 85. Values used in the present work taken from supplement issued in 1970.

[6]G. A. Harrower, Rev. Sci. Instrum. 26, 850 (1955).
[7]D. H. Crandall, J. A. Ray, and C. Cisneros, Rev. Sci. Instrum. 46, 562 (1975).
[8]G. W. McClure, Phys. Rev. 130, 1852 (1963); J. W. McGowan and L. Kerwin, Can. J. Phys. 42, 972 (1964).
[9]J. F. Williams and D. N. F. Dunbar, Phys. Rev. 149, 62 (1966).
[10]M. A. D. Fluendy and K. P. Lawley, *Chemical Applications of Molecular Beam Scattering* (Chapman and Hall, London, 1978), pp. 37–44.
[11]Ramiro García G., A. Rossi, and A. Russek (unpublished).
[12]H. Inouye, K. Niurao, and S. Kita, Chem. Phys. Lett. 33, 241 (1975).